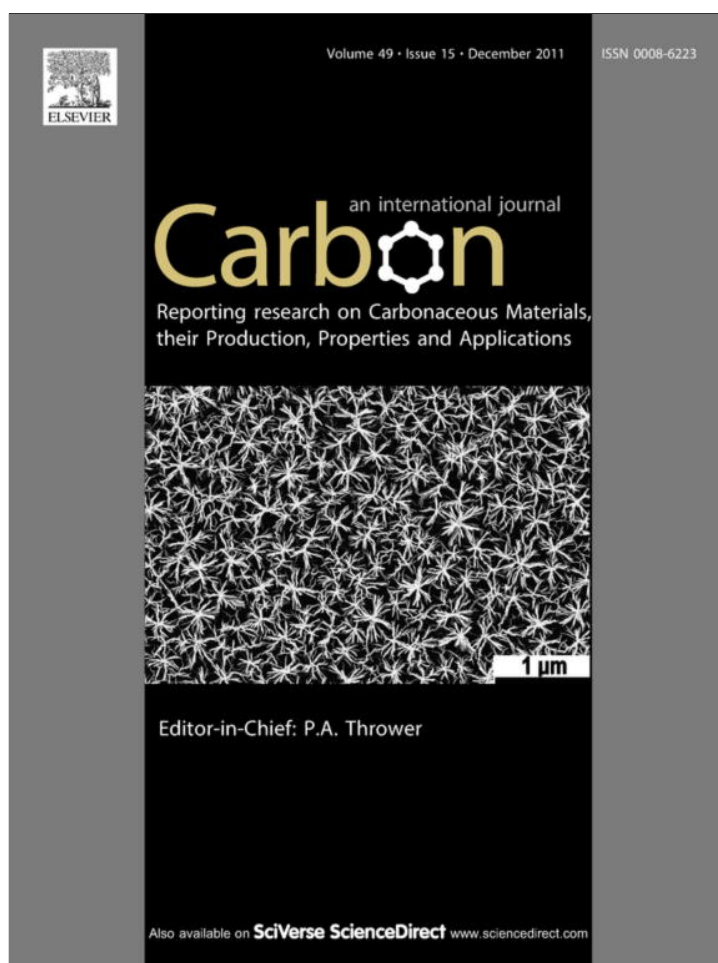


Provided for non-commercial research and education use.
Not for reproduction, distribution or commercial use.



This article appeared in a journal published by Elsevier. The attached copy is furnished to the author for internal non-commercial research and education use, including for instruction at the authors institution and sharing with colleagues.

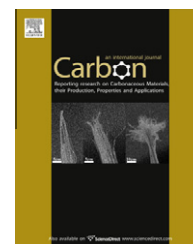
Other uses, including reproduction and distribution, or selling or licensing copies, or posting to personal, institutional or third party websites are prohibited.

In most cases authors are permitted to post their version of the article (e.g. in Word or Tex form) to their personal website or institutional repository. Authors requiring further information regarding Elsevier's archiving and manuscript policies are encouraged to visit:

<http://www.elsevier.com/copyright>

Available at www.sciencedirect.com

SciVerse ScienceDirect

journal homepage: www.elsevier.com/locate/carbon

Synthesis and characterization of phosphorus–nitrogen doped multiwalled carbon nanotubes

Jian Liu ^a, Hao Liu ^a, Yong Zhang ^a, Ruying Li ^a, Guoxian Liang ^b, Michel Gauthier ^b, Xueliang Sun ^{a,*}

^a Department of Mechanical and Materials Engineering, University of Western Ontario, London, ON, Canada N6A 5B9

^b Phostech Lithium Inc., 1475, rue Marie-Victorin, St-Bruno, QC, Canada J3V 6B7

ARTICLE INFO

Article history:

Received 9 March 2011

Accepted 12 July 2011

Available online 21 July 2011

ABSTRACT

Phosphorus–nitrogen doped multiwalled carbon nanotubes (CN_xP_y) were prepared using a floating catalyst chemical vapor deposition method. Triphenylphosphine (TPP), as phosphorus (P) precursor, was used to control the structure of the CN_xP_y. Transmission electron microscope (TEM) observation indicated that with the increase of TPP amount, the outer diameter and wall thickness of the CN_xP_y gradually increased, while their inner diameter decreased. TEM and backscattered electron imaging revealed that structural changes of the nanotubes could be attributed to the shape change of the catalyst particles, from conical for nitrogen-doped carbon nanotubes (CN_x) to elongated for CN_xP_y, with the addition of TPP. X-ray photoelectron spectroscopy analysis demonstrated that the P content in CN_xP_y can reach as high as 1.9 at.%. Raman analysis indicated that CN_xP_y had a lower crystallinity than CN_x.

© 2011 Elsevier Ltd. All rights reserved.

1. Introduction

Carbon nanotubes (CNTs) [1] have been widely studied by scientists all over the world in the last two decades, due to their outstanding mechanical properties, electrical conductivity, and thermal stability [2–4]. These properties not only inspire fundamental studies on CNTs, such as band structure and chirality [5], but also make CNTs a potential candidate for a wide range of applications, such as semiconductor probes and interconnects, field emission display sources, and energy storage and conversion devices [6,7]. Recently, there has been a great interest in controlling and improving the properties of CNTs through different functionalization methods, among which doping CNTs with foreign atoms has been proven to be an effective approach [8]. For example, nitrogen (N) atoms can donate additional electrons to the delocalized π system of the hexagonal carbon framework. Thus nitrogen-doped CNTs (CN_x) exhibit improved electrical conductivity, compared with its non-doped counterpart [9]. The oxidation resistance of

CNTs can be decreased by doping N, which introduces high-reactivity defects along nanotubes, or increased by doping boron (B), which poisons carbon active sites or forms B₂O₃ film on the surface of nanotubes protecting them from oxidation [10]. Hence, doping has been considered as a feasible strategy in a well-defined way to modify the physical and chemical properties of CNTs.

In addition to N and B, which have been intensively studied for doping in CNTs, phosphorus (P) is another doping element to modify the structure and properties of CNTs. However, studies on P doping are seldom reported. An early study on P doped diamond-like carbon (DLC) has shown that P doping could improve the electrical character of DLC by reducing the turn-on voltage and increasing the emission current density [11]. P doping in singlewalled carbon nanotubes (SWNTs) has been studied both theoretically and experimentally [12–14]. The experimental results show that P doping can significantly change the optical transition absorptions [12] and thermal conductivity of SWNTs [13]. A density functional

* Corresponding author: Fax: +1 519 661 3020.

E-mail address: xsun@uwo.ca (X. Sun).

0008-6223/\$ - see front matter © 2011 Elsevier Ltd. All rights reserved.

doi:10.1016/j.carbon.2011.07.018

theory (DFT) study on P doped SWNTs demonstrates that substitutional P can create localized electronic states that modify the electron transport properties of SWNTs by acting as scattering centers [14]. In addition, the substitutional P doping also alters the mechanical strength of SWNTs, leading to a 50% reduction in the elongation upon fracture [14].

Recently, phosphorus-nitrogen doped multiwalled carbon nanotubes (CN_xP_y) were synthesized by a spray pyrolysis method [15]. In this process, iron phosphide (Fe_3P) acted as the catalyst for the growth of nanotubes. Electron energy loss spectroscopy analysis demonstrated that P and N were homogeneously incorporated into the lattice of nanotubes, changing the chemical properties of CN_xP_y [15]. Nevertheless, it is still challenging to synthesize high-content P doped CNTs, while high-content N or B doped CNTs have already been achieved [16,17]. The reason is partially due to the large atomic radius difference between C (0.77 Å) and P (1.10 Å), compared with that between C and N (0.74 Å) or B (0.88 Å) [18]. This large difference would greatly increase the disorder within the hexagonal carbon framework, thus making P difficult to be doped in CNTs. However, DFT simulation demonstrated that P–N defects exhibited lower formation energy (by ca. 0.45 eV) than P defects in nanotubes [15]. In other words, by doping P and N in CNTs at the same time, it is possible to obtain a higher P content than that obtained by doping P alone. Furthermore, Ghosh et al. [16] recently reported that CN_x with a N content of 25.7 at.% were prepared by a catalytic chemical vapor deposition method using imidazole as N precursor. Therefore, a high P content can be expected in CN_xP_y , when imidazole and Triphenylphosphine (TPP), as N and P precursor respectively, are used at the same time. Meanwhile, the bonding environment of P plays a role as important as P content in determining the properties of CN_xP_y . However, it has not been reported in previous literature.

In our present work, CN_xP_y with a P content of 1.9 at.%, the highest reported so far, are synthesized by a floating catalyst chemical vapor deposition (FCCVD) method using ferrocene, imidazole and TPP as precursors. The effect of the amount of TPP on the structure of CN_xP_y is studied. A growth mechanism of CN_xP_y is proposed based on our observation. Moreover, bonding environments of P in CN_xP_y are also examined, and possible bonding forms of P in CN_xP_y are discussed.

2. Experimental

A silicon wafer coated with an aluminum buffer layer (30 nm thickness) was used as a substrate for the growth of CN_x and CN_xP_y . The aluminum buffer layer can significantly improve the quality and growth rate of CNTs by helping the formation of uniform and well-dispersed catalyst particles on the surface of the substrate [19]. The aluminum buffer layer was coated on the surface of the silicon wafer in a sputtering system operated under a pressure of 4.0 mTorr and at a power of 300 W.

FCCVD method [19,20] was applied to synthesize CN_x and CN_xP_y in a horizontal quartz tube furnace system. Two grams of imidazole ($C_3H_4N_2$, Alfa Aesar, 99%) was thoroughly mixed with different amounts (10, 30 and 50 mg) of TPP ($P(C_6H_5)_3$,

Aldrich, 99%). Then the mixture was put into a small quartz container. Ten milligrams of ferrocene ($Fe(C_5H_5)_2$, Aldrich, 98%) was put into a holder, which was placed over the quartz container to keep ferrocene and the mixture separate. A small piece of the substrate described above was placed in the center of the quartz tube. Before the furnace was heated, argon (Ar) gas (99.999% in purity) was introduced into the quartz tube at a flow rate of 500 sccm for 10 min in order to expel the air in the quartz tube. After that, the system was heated to 850 °C at a rate of 60 °C/min. Then the quartz container was pushed into a location near the entrance of the furnace first, where the temperature was around 100 °C, suitable for the liquefaction of the mixture of imidazole and TPP. Once all the mixture was liquefied, the quartz container was pushed further into the entrance of the furnace, where the temperature was around 200 °C. At this point, ferrocene and the mixture of imidazole and TPP evaporated simultaneously. The vapor of all chemicals was brought into the high temperature region by the Ar gas where the pyrolysis and synthesis occurred at 850 °C. This step lasted for 10 min. At last, the furnace was turned off and cooled down to room temperature in the flowing Ar gas.

Morphologies of these samples were characterized by Hitachi S-4800 field-emission scanning electron microscope (SEM) operated at 5 kV, Philips CM10 transmission electron microscope (TEM) operated at 80 kV, and JEOL 2010 FEG high-resolution TEM (HRTEM). Composition and element analyses of these samples were carried out by Kratos Axis Ultra Al (alpha) X-ray photoelectron spectrometer (XPS) operated at 14 kV. Raman spectra of these samples were examined by a HORIBA Scientific LabRAM HR800 Raman spectrometer with an incident laser beam of 532.4 nm.

3. Results and discussion

3.1. Structural characterization of CN_xP_y

Fig. 1(a–d) shows typical SEM images of CN_x and CN_xP_y obtained with different amounts of TPP. It can be seen that CN_x and CN_xP_y grew perpendicularly to the silicon wafer with different densities and thicknesses of the CNT layer. As seen in Fig. 1(a), the silicon wafer is totally covered by aligned CN_x with high density. The thickness of the CNT layer was measured to be about 42 μm for CN_x . When TPP is used in the synthesis process, the shape of these nanotubes experiences an obvious change from curved for CN_x to straight for CN_xP_y . The thickness of the CNT layer decreases from 42 μm for CN_x to 29, 13 and 12 μm for CN_xP_y synthesized with 10, 30 and 50 mg of TPP respectively, as seen in Fig. 1(b–d). And the density of these nanotubes also experiences a decrease with the increase of TPP amount. These results indicate that the growth of nanotubes is greatly suppressed by the addition of TPP. This phenomenon was also observed previously [15], in which the catalyst activity gradually deteriorated due to the increasing ratio of Fe_2P to Fe_3P in the catalyst with the addition of TPP and finally hampered the growth of CN_xP_y .

In order to investigate the relationship between the structure of CN_xP_y and the amount of TPP used, TEM characterization was carried out, and the result is presented in Fig. 2.

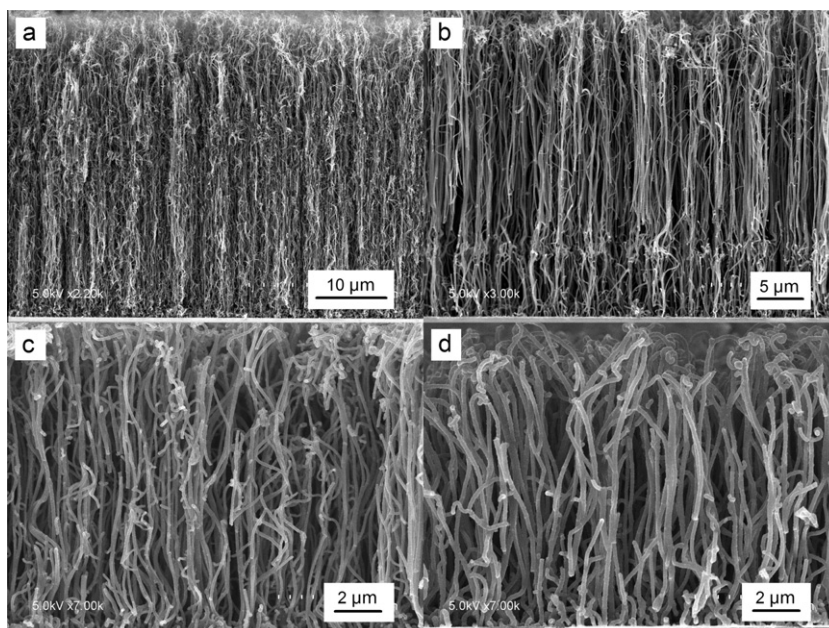


Fig. 1 – SEM images of CN_x (a) and CN_xP_y synthesized with 10 mg (b), 30 mg (c), and 50 mg (d) of TPP.

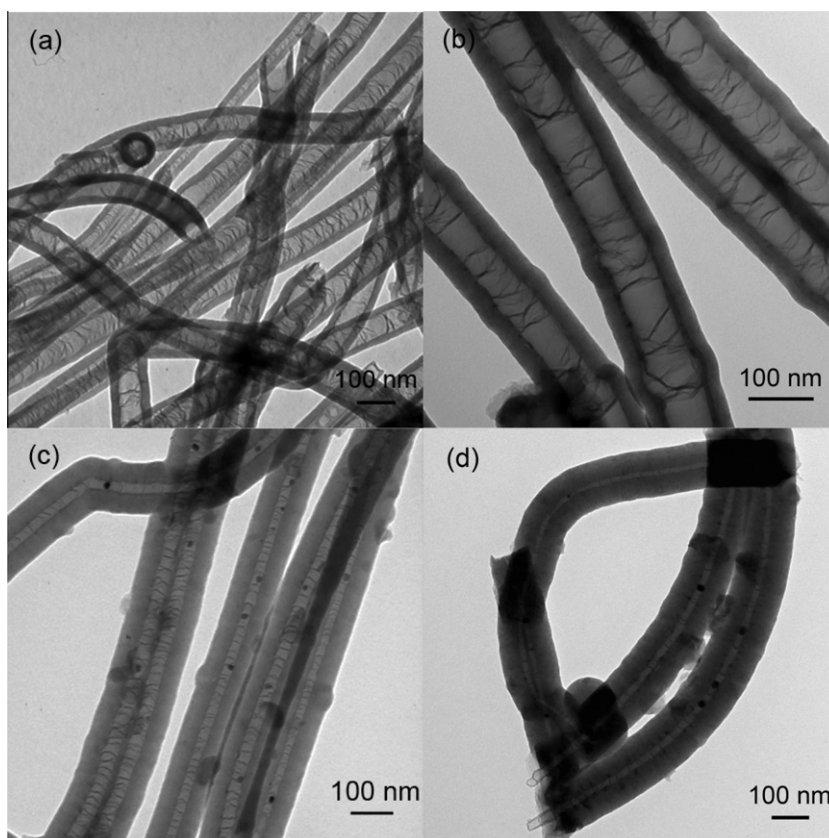


Fig. 2 – TEM images of CN_x (a) and CN_xP_y synthesized with 10 mg (b), 30 mg (c), and 50 mg (d) of TPP.

Fig. 2(a) shows a typical TEM image of CN_x synthesized without TPP. It can be seen that CN_x exhibit an irregular and inter-linked corrugated structure, which is typical for CN_x. With the addition of TPP, all CN_xP_y show similarities in the inner structure to CN_x, which looks like many cones stacked together.

But great differences can be observed between CN_x and CN_xP_y in their outer diameters and wall thicknesses. The ratio between the inner and the outer diameter (D_i/D_o) of CN_x or CN_xP_y is used to show the variation of wall thickness. At least 100 nanotubes were measured to calculate the average value

of D_i/D_o of CN_x and each kind of CN_xP_y . The outer diameter of CN_x is around 70–90 nm, and the wall thickness is around 15–35 nm, as seen in Fig. 2(a). So D_i/D_o is around 0.68 for CN_x . When 10 mg of TPP is added to the reaction, the outer diameter and the wall thickness of CN_xP_y increase to 110–130 nm and 60–70 nm respectively, while D_i/D_o decreases to around 0.48, as shown in Fig. 2(b). With 30 mg of TPP, the outer diameter of CN_xP_y stays almost unchanged, whereas the wall thickness increases to 80–100 nm. D_i/D_o drops to 0.23. When the amount of TPP is further increased to 50 mg, the outer diameter and the wall thickness of CN_xP_y increase to 150–160 nm and 120–140 nm respectively. D_i/D_o stays almost unchanged at around 0.22. These results suggest that the structure of CN_xP_y can be controlled by changing the amount of TPP used in the reaction. With the increasing amount of TPP, the outer diameter and the wall thickness of CN_xP_y increase, while the inner diameter decreases greatly. Interestingly, it is found that a few small catalyst particles with a spherical shape are trapped in the inner nanotubes of CN_xP_y synthesized with 30 and 50 mg of TPP.

In order to understand the effect of TPP on the structural changes of CN_xP_y , backscattered electron (BSE) imaging and TEM were performed on CN_x and CN_xP_y synthesized with 30 mg of TPP, focusing on their catalyst particles. From BSE images, Fig. 3(a) and (b), it can be clearly seen that catalyst particles are located at the bottom of nanotubes for both CN_x and CN_xP_y . This phenomenon suggests that the growth of CN_x and CN_xP_y follow a base-growth mechanism. This is consistent with the root growth model for CN_xP_y as reported by Sumpter et al. [21]. In Fig. 3, it can also be found that there are great differences between CN_x and CN_xP_y in the shape and the size of catalyst particles. The catalyst particles of CN_x

have a conical shape, and their sizes are around 50–60 nm. In comparison, the catalyst particles of CN_xP_y are elongated, and the sizes of their top and bottom are about 20–40 nm and 70–90 nm respectively. These results are further confirmed by TEM observations, as shown in Fig. 3(c) and (d). In Fig. 3(a–d), it can be found that for both CN_x and CN_xP_y , the inner diameter of nanotubes is related to the size of the catalyst top. Previous studies have shown that the inner layer of CN_x or CN_xP_y is formed from the top surface of the catalysts through bulk diffusion, while the outer layer of CN_x or CN_xP_y is nucleated from the side of the catalyst mainly through surface diffusion [22,23]. Therefore, the inner diameter of nanotubes depends on the size of the catalyst top. Hence, in our case, the smaller inner diameter of CN_xP_y than CN_x could be attributed to the smaller top surface of the elongated catalyst than the conical one. The shape and size difference between the catalyst of CN_x and that of CN_xP_y is probably due to their different melting points. The Fe_2P or Fe_3P catalysts for CN_xP_y has a lower melting point (MP) (1166 °C for Fe_3P , 1370 °C for Fe_2P) than pure Fe (1538 °C) for CN_x [15,24]. During the process of nanotube growth, catalyst particles with a low MP would be easily deformed and elongated along the direction of nanotube growth due to the extrusion force caused by nanotube precipitation [22]. Thus it is reasonable to believe that the top of elongated catalyst particles can be separated by the extrusion force occasionally, forming small particles trapped in the inner nanotubes observed in Fig. 2(c) and (d). It is noticed that similar sequential trapping of catalyst particles in CNTs was also previously observed by Jourdain et al., and it was due to the inclusion of P into the catalyst particles [25]. The growth mechanisms for CN_x and CN_xP_y are shown in Fig. 3(e).

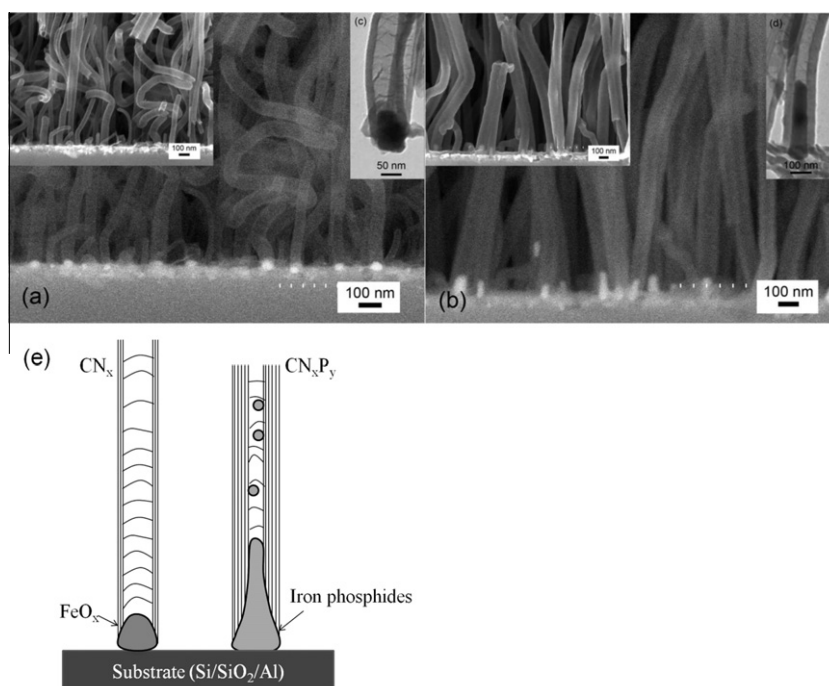


Fig. 3 – BSE images of CN_x (a) and CN_xP_y synthesized with 30 mg of TPP (b), and corresponding SEM images are inserted on the up-left corner of BSE images. Typical TEM images of an individual nanotube for CN_x (c) and CN_xP_y synthesized with 30 mg of TPP (d). Schematic diagram of growth mechanisms for CN_x and CN_xP_y (e).

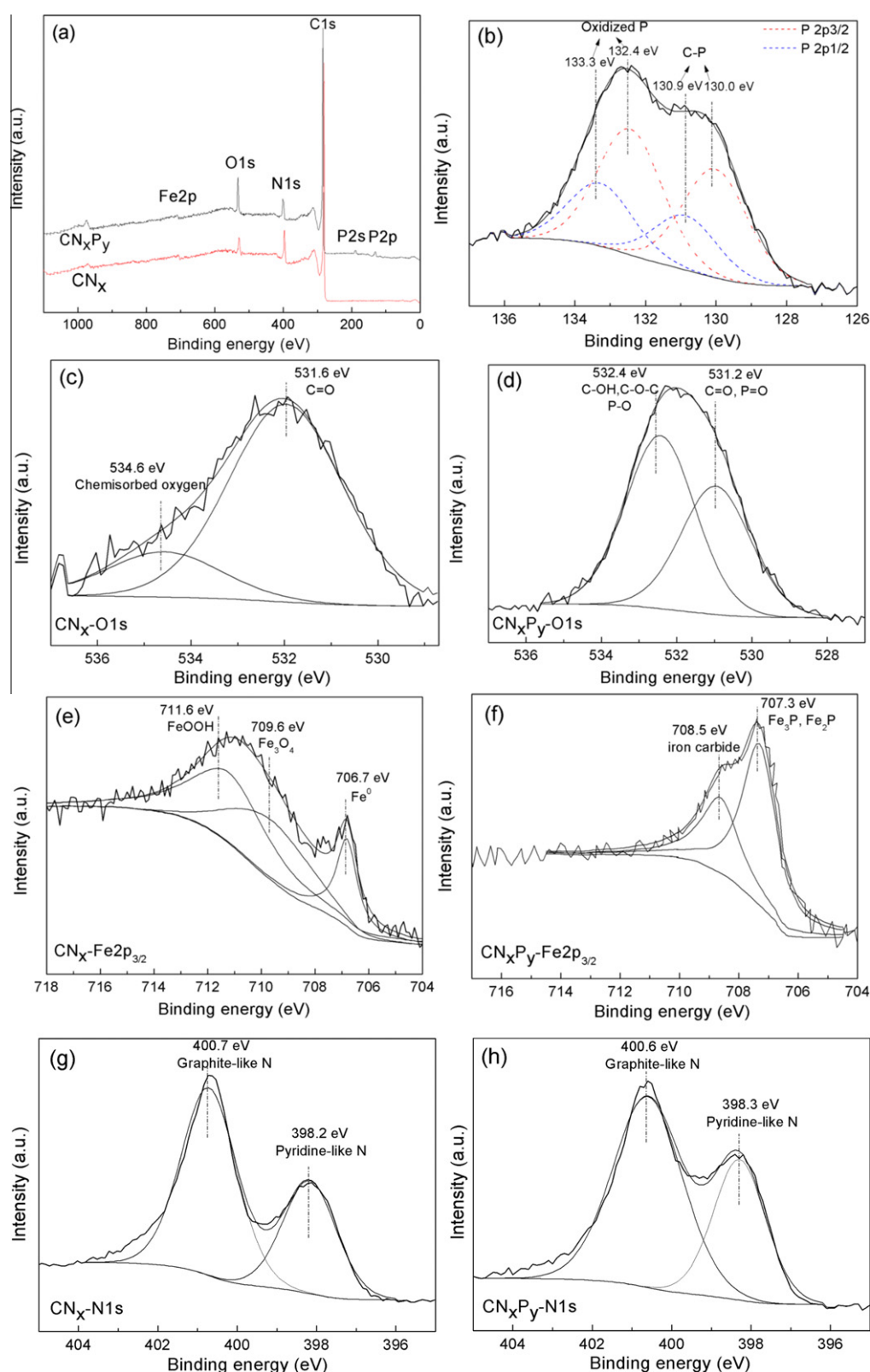


Fig. 4 – XPS survey scan spectra of CN_xP_y synthesized with 50 mg of TPP and CN_x (a), deconvolution of P2p (if applicable), O1s, $\text{Fe}2p_{3/2}$ and N1s peaks for CN_xP_y synthesized with 50 mg of TPP (b, d, f, h) and CN_x (c, e, g).

3.2. Bonding environments of P in CN_xP_y

In order to determine P content and its bonding environments in CN_xP_y , XPS was performed on CN_xP_y synthesized with

50 mg of TPP, and the result is shown in Fig. 4. For comparison, the XPS result of CN_x is also given out. Fig. 4(a) shows full-range XPS spectra of CN_x and CN_xP_y synthesized with 50 mg of TPP. For CN_x , the main peaks are distinguished at

280.9 eV, 396.35 eV, 528.7 eV and 705.8 eV, corresponding to C1s, N1s, O1s, and Fe2p, respectively. For CN_xP_y , besides the elements above, the existence of P is indicated by the two peaks located at 131.1 eV and 188.9 eV, which are P2p and P2s respectively. The content of P, defined as atomic percent of P with respect to the sum of C and P, is estimated by the area ratio of P peak and the sum of P and C peaks ($P/(C + P)$). The P content of CN_xP_y is calculated to be 1.9 at.%. Because the catalyst particles of CN_xP_y are P-rich [15], their contribution to total P content should also be considered. The deconvolution of Fe2p_{3/2} peaks for CN_x and CN_xP_y are shown in Fig. 4(e) and (f), respectively. For CN_x , the Fe2p_{3/2} peak is fitted into Fe⁰, Fe₃O₄ and FeOOH, located at 706.7, 709.6 and 711.6 eV respectively [19]. For CN_xP_y , the Fe2p_{3/2} peak is fitted into two components 707.3 and 708.5 eV respectively. The first component corresponds to Fe₂P or Fe₃P [26], and the second one is for iron carbide [27], with their respective contributions of 64.3% and 35.7%. Fe/P ratio of CN_xP_y is determined to be 0.19. Therefore, Fe₂P or Fe₃P in catalyst particles contributes 4–6% to the total P content of CN_xP_y . The asymmetric P2p peak is fitted into two double peaks, as seen in Fig. 4(b). The first two peaks near 130.0 eV indicate the presence of C–P bonds [28], and the second two ones around 133.0 eV are associated with oxidized P [28,29]. It is reasonable to think that a fraction of P at the nanotube surface was oxidized during the synthesis process because of the presence of oxygen, which can be attributed to several reasons, such as the oxygen released from solid precursors and the oxygen adsorbed on the surface of the substrate [30]. However, the O/P ratio is as high as 4.3 for CN_xP_y , implying that oxidized P only contribute a small fraction to the O1s peak. The oxidized P probably exists as P–O or P=O bonds [28,29] as seen in Fig. 4(d).

N doping is an important factor to determine the properties of CNTs. Therefore, the effect of TPP addition on the N content and N bonding environments in CN_xP_y is studied. The N content, defined as atomic percent of N with respect to the sum of C and N, is estimated by the area ratio of N peak and the sum of C and N peaks ($N/(C + N)$). With the addition of TPP, the N content decreases from 10.2 at.% for CN_x to 7.1 at.% for CN_xP_y . The deconvolution of N1s peaks for CN_x and CN_xP_y is shown in Fig. 4(g) and (h) respectively. It can be seen that, for both samples, N1s peak is fitted into two peaks at 400.6 eV and 398.3 eV, which correspond to graphite-like N and pyridine-like N respectively [20]. The intensity ratio between graphite-like N and pyridine-like N (I_{GN}/I_{PN}) is 1.7 for CN_xP_y and 1.8 for CN_x . These results indicate that the addition of TPP may suppress the doping of N into CN_xP_y , but has little effect on the types of N.

3.3. Crystallinity of CN_xP_y

To obtain information about the effect of TPP addition on the crystallinity of CN_xP_y , HRTEM and Raman spectra were performed on CN_x and CN_xP_y synthesized with 50 mg of TPP. The HRTEM images of CN_x and CN_xP_y are shown in Fig. 5. CN_xP_y have very thick nanotube walls (as seen in Fig. 2(d)), which make it difficult to obtain information about the inner nanotubes by HRTEM. Thus we only compare the features of the outer surfaces of CN_x and CN_xP_y . In Fig. 5, it can be seen that both CN_x and CN_xP_y have rough surfaces with a thin

amorphous layer. Compared with CN_x , CN_xP_y exhibit a slight decrease in the degree of long-range ordered crystallinity.

Two first-order Raman spectra of CN_xP_y synthesized with 50 mg of TPP and CN_x were plotted in Fig. 6. The band located at $\sim 1342\text{ cm}^{-1}$ (D-band) is originated from atomic displacement and disorder induced features caused by lattice defect, distortion, or the finite particle size [31]. The band at ~ 1568 to 1582 cm^{-1} (G-band) indicates the formation of well-graphitized CNTs [32]. The intensity ratio between D-band and G-band (I_D/I_G) or the variation of the full width at half-maximum (FWHM) is usually used to represent the crystalline order in CNTs [20,10,33]. In our case, I_D/I_G is calculated to be 0.94 for both CN_x and CN_xP_y . The FWHMs of D-band and G-band increase from 146.3 and 83.6 cm^{-1} for CN_x to 161.2 and 101.5 cm^{-1} for CN_xP_y respectively. Narrowing of the Raman modes indicates a better crystallization of the nanotubes or a larger crystal planer domain size in graphite sheets and consequently a lower degree of disorder [33]. In our case, the broadening of D-band and G-band of CN_xP_y shows that they have a lower crystalline order than CN_x . This is in accordance with the HRTEM result. Therefore, it can be concluded

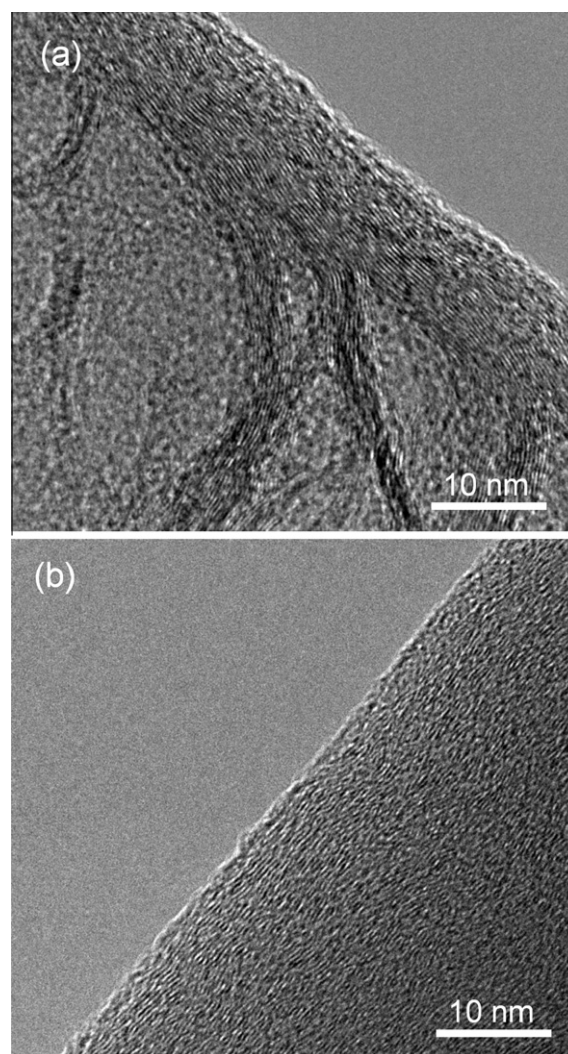


Fig. 5 – HRTEM images of CN_x (a) and CN_xP_y synthesized with 50 mg of TPP (b).

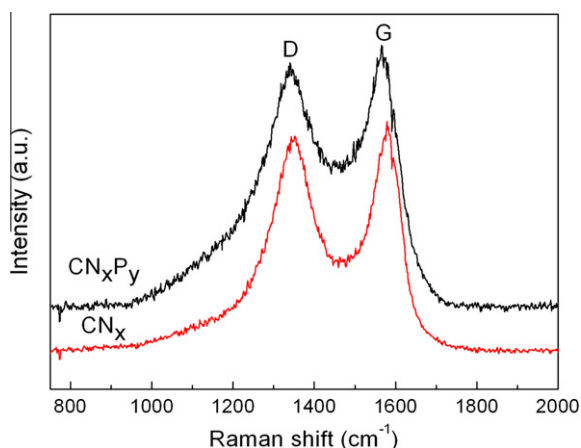


Fig. 6 – Raman spectra of CN_x and CN_xP_y , synthesized with 50 mg of TPP.

that the addition of TPP during synthesis process leads to a lower crystallinity of CN_xP_y than CN_x . It is well known that the decrease of N content in CN_x usually leads to an increase of crystalline order [20,10]. However, in our case, CN_xP_y still exhibit a lower crystalline order than CN_x , although the N content of the former (7.1 at.%) is lower than that of the latter (10.2 at.%). The reason is probably due to the P doping into CN_xP_y by introducing TPP. A previous study has shown that the incorporation of P into SWNTs can cause a substantial increase in D-band intensity [12], which suggests an increase in defects and disorder. Therefore, it can be considered that P doping contributes to an increase in defects and disorder in CN_xP_y . The P and N doping result in a lower crystalline order of CN_xP_y than that of CN_x . Moreover, it is noticed that G-band undergoes a down-shift from 1582 cm^{-1} for CN_x to 1568 cm^{-1} for CN_xP_y . The G-band represents the tangential mode vibration of carbon atoms in graphene sheets, and shifts of the G-band are interpreted in terms of C–C expansion (or contraction) and the changes of electronic structure [32]. The down-shift of G-band could also be attributed to the P doping in CN_xP_y . P atoms can provide more free electrons than N atoms do. Both N and P in CN_xP_y can act as electron donors, and improve electron transfer between valance and conduction bands.

4. Conclusions

Aligned phosphorus–nitrogen doped multiwalled carbon nanotubes (CN_xP_y) with tunable structure have been synthesized on a silicon wafer by a simple FCCVD method. SEM analysis showed that the length and yield of CN_xP_y decreased dramatically with an increase in the amount of TPP. TEM observations indicated that with an increasing amount of TPP, the outer diameter and the wall thickness of CN_xP_y gradually increased, while the inner diameter decreased, represented by the decrease of D_i/D_o from 0.68 for CN_x , to 0.48, 0.23 and 0.22 for CN_xP_y with TPP amount of 10, 30 and 50 mg, respectively. TEM and BSE imaging studies revealed that the shape changes of catalyst particles, from conical for CN_x to elongated for CN_xP_y , was responsible for these structural changes. XPS result revealed that CN_xP_y had a P

content of 1.9 at.%, with 4–6% contribution from the P-rich catalyst particles. The P in CN_xP_y existed in C–P bonds, and part of P at the nanotube surface was oxidized. Raman analysis showed CN_xP_y exhibited broader FWHM for both the G-band and D-band, and a lower position of the G-band than for CN_x due to P doping. Both XPS and HRTEM results indicate that CN_xP_y was less crystalline than CN_x .

Acknowledgements

This research was supported by Natural Sciences and Engineering Research Council of Canada (NSERC), Phostech Lithium Inc., Canada Research Chair (CRC) Program, Canada Foundation for Innovation (CFI), Ontario Research Fund (ORF), Ontario Early Researcher Award (ERA) and University of Western Ontario. We are in debt to David Tweddell, Fred Pearson, Ronald Smith and Mark Biesinger for their kind help and fruitful discussions.

REFERENCES

- [1] Iijima S. Helical microtubules of graphitic carbon. *Nature* 1991;354(6348):56–8.
- [2] Dresselhaus M, Dresselhaus G, Saito R. Physics of carbon nanotubes. *Carbon* 1995;33(7):883–91.
- [3] Grobert N. Carbon nanotubes-becoming clean. *Mater Today* 2007;10(1–2):28–35.
- [4] Okamoto A, Gunjishima I, Inoue T, Akoshima M, Miyagawa H, Nakano T, et al. Thermal and electrical conduction properties of vertically aligned carbon nanotubes produced by water-assisted chemical vapor deposition. *Carbon* 2011;49:294–8.
- [5] Antram MP, Léonard F. Physics of carbon nanotube electronic devices. *Rep Prog Phys* 2006;69:507–61.
- [6] Baughman RH, Zakhidov AA, De Heer WA. Carbon nanotubes-the route toward applications. *Science* 2002;297(2):787–92.
- [7] Gong K, Du F, Xia Z, Durstock M, Dai L. Nitrogen-doped carbon nanotube array with high electrocatalytic activity for oxygen reduction. *Science* 2009;323:760–4.
- [8] Ayala P, Arenal R, Rummeli M, Rudio A, Pichler T. The doping of carbon nanotubes with nitrogen and their potential applications. *Carbon* 2010;48:575–86.
- [9] Terrones M, Ajayan PM, Banhart F, Blasé X, Carrol DL, Charlier JC, et al. N-doped and coalescence of carbon nanotubes: synthesis and electronic properties. *Appl Phys A* 2002;74:355–61.
- [10] Koós AA, Dillon F, Obraztsova EA, Crossley A, Grobert N. Comparison of structural changes in nitrogen and boron-doped multi-walled carbon nanotubes. *Carbon* 2010;48:3033–41.
- [11] Chen CF, Tsai CL, Lin CL. Electronic properties of phosphorus-doped triode-type diamond field emission arrays. *Mater Chem Phys* 2001;72:210–3.
- [12] Xu J, Guan L. Diameter-selective band structure modification of single-walled carbon nanotubes by encapsulated phosphorus chains. *J Phys Chem C* 2009;113(34):15099–101.
- [13] Maciel IO, Campos-Delgado J, Cruz-Silva E, Pimenta MA, Sumpter BG, Meunier V, et al. Synthesis, electronic structure, and Raman scattering of phosphorus-doped single-wall carbon nanotubes. *Nano Lett* 2009;9(6):2267–72.
- [14] Cruz-Silva E, López-Uías F, Muñoz-Sandoval E, Sumpter BG, Terrones H, Charlier JC, et al. Electronic transport and

- mechanical properties of phosphorus- and phosphorus-nitrogen-doped carbon nanotubes. *ACS Nano* 2009;3(7):1913–21.
- [15] Cruz-Silva E, Cullen DA, Gu L, Romo-Herrera JM, Munoz-Sandoval E, López-Uías F, et al. Heterodoped nanotubes: theory, synthesis, and characterization of phosphorus-nitrogen doped multiwalled carbon nanotubes. *ACS Nano* 2008;2(3):441–8.
- [16] Ghosh K, Kumar M, Maruyama T, Ando Y. Controllable growth of highly N-doped carbon nanotubes from imidazole: structural, spectroscopic and field emission study. *J Mater Chem* 2010;20:4128–34.
- [17] Redlich PH, Loeffler J, Ajayan PM, Bill J, Aldinger F, Rühle M. B–C–N nanotubes and boron doping of carbon nanotubes. *Chem Phys Lett* 1996;260:465–70.
- [18] Rossotti H. *Diverse atoms: profiles of the chemical elements*. New York: Oxford University Press; 1998. p. 62–158.
- [19] Liu H, Arato D, Li R, Zhang Y, Merel P, Sun X. Aligned multiwalled carbon nanotubes synthesized by floating catalyst CVD: effects of buffer layer and substrates. *Surf Coating Tech* 2008;202(17):4114–20.
- [20] Liu H, Zhang Y, Li R, Sun X, Désilets S, Abou-Rachid H, et al. Structural and morphological control of aligned nitrogen-doped carbon nanotubes. *Carbon* 2010;48:1498–507.
- [21] Sumpter BG, Huang J, Meunier V, Romo-Herrera JM, Cruz-Silva E, Terrones H, et al. A theoretical and experimental study on manipulating the structure and properties of carbon nanotubes using substitutional dopants. *Int J Quantum Chem* 2009;109:97–118.
- [22] Reyes-Reyes M, Grobert N, Kamalakaran R, Seeger T, Golberg D, Rühle M, et al. Efficient encapsulation of gaseous nitrogen inside carbon nanotubes with bamboo-like structure using aerosol thermolysis. *Chem Phys Lett* 2004;396:167–73.
- [23] Lee CJ. Growth model of bamboo-shaped carbon nanotubes by thermal chemical vapor deposition. *Appl Phys Lett* 2000;77(21):3397–9.
- [24] Benissad-Aissani F, Ait-Amar H, Schouler MC, Gabelle P. The role of phosphorus in the growth of vapour-grown carbon fibres obtained by catalytic decomposition of hydrocarbons. *Carbon* 2004;32:2163–8.
- [25] Jourdain V, Simpson ET, Paillet M, Kasama T, Dunin-Borkowski RE, Poncharal P, et al. Periodic inclusion of room-temperature-ferromagnetic metal phosphides nanoparticles in carbon nanotubes. *J Phys Chem B* 2006;110(20):9759–63.
- [26] Godec M, Mandrino DJ, Šuštaršič, Nolan D, Jenko M. Characterization of rapidly solidified nanocrystalline soft magnetic ribbons based on Fe–Si–B with P and Ga additions. *Surf Interface Anal* 2008;40:498–502.
- [27] Bonnet F, Ropital F, Berthier Y, Marcus P. Filamentous carbon formation caused by catalytic metal particles form iron oxide. *Mater Corros* 2003;54(11):870–80.
- [28] Gorham J, Torres J, Wolfe G, d'Agostino A, Fairbrother DH. Surface reactions of molecular and atomic oxygen with carbon phosphide films. *J Phys Chem B* 2005;109:20379–86.
- [29] Puziy AM, Poddubnaya OI, Socha RP, Gulgul J, Wisniewski M. XPS and NMR studies of phosphoric acid activated carbons. *Carbon* 2008;46:2113–23.
- [30] He M, Zhou S, Zhang J, Liu Z, Robinson C. CVD growth of N-doped carbon nanotubes on silicon substrates and its mechanism. *J Phys Chem B* 2005;109(19):1808–20.
- [31] Choi H, Park J, Kim B. Distribution and structure of N atoms in multiwalled carbon nanotubes using variable-energy X-ray photoelectron spectroscopy. *J Phys Chem B* 2005;109:4333–40.
- [32] Dresselhaus MS, Dresselhaus G, Saito R, Jorio A. Raman spectroscopy of carbon nanotubes. *Phys Rep* 2005;409(2):47–99.
- [33] Yadav RM, Dobal PS, Shripathi T, Katiyar RS, Srivastava ON. Effect of growth temperature on bamboo-shaped carbon–nitrogen (C–N) nanotubes synthesized using ferrocene acetonitrile precursor. *Nanoscale Res Lett* 2009;4:197–203.